Theoretical study on mechanism of the photochemical ligand substitution of *fac*-$[Re^{I}(bpy)(CO)_3(PR_3)]^+$ complex

Kenichiro Saita,[*a] Yu Harabuchi[a], Tetsuya Taketsugu[a], Osamu Ishitani[b] and Satoshi Maeda[*a]

[a] *Department of Chemistry, Faculty of Science, Hokkaido University, Kita 10, Nishi 8, Kita-ku, Sapporo 060-0810, Japan*

[b] *Department of Chemistry, Graduate School of Science and Engineering, Tokyo Institute of Technology, O-okayama 2-12-1, NE-1, Meguro-ku, Tokyo 152-8551, Japan*

* Corresponding authors. Tel./Fax.: +81 11 706 4921 (KS, SM).

E-mail address: ksaita@mail.sci.hokudai.ac.jp (KS), smaeda@mail.sci.hokudai.ac.jp (SM).

Abstract

The mechanism of the CO ligand dissociation of *fac*-[Re^{I}(bpy)$(CO)_3P(OMe)_3]^+$ has theoretically been investigated, as the dominant process of the photochemical ligand substitution (PLS) reactions of *fac*-[Re^{I}(bpy)$(CO)_3PR_3]^+$, by using the (TD-)DFT method. The PLS reactivity can be determined by the topology of the T_1 potential energy surface, since the photoexcited complex is able to decay into the T_1 state by internal conversions (through conical intersections) and intersystem crossings (via crossing seams) with sufficiently low energy barriers. The T_1 state has a character of the metal-to-ligand charge-transfer (^{3}MLCT) around the Franck-Condon region, and it changes to the metal-centered (^{3}MC) state as the Re-CO bond is elongated and bent. The equatorial CO ligand has a much higher energy barrier to leave than that of the axial CO, so that the axial CO ligand selectively dissociates in the PLS reaction. The single-component artificial force induced reaction (SC-AFIR) search reveals the CO dissociation pathway in photostable *fac*-[Re^{I}(bpy)$(CO)_3$Cl] as well, however, the dissociation barrier on the T_1 state is substantially higher than that in *fac*-[Re^{I}(bpy)$(CO)_3PR_3]^+$ and the minimum-energy seams of crossings (MESXs) are located before and below the barrier. The MESXs have also been searched in *fac*-[Re^{I}(bpy)$(CO)_3PR_3]^+$ and no MESXs were found before and below the barrier.

1. Introduction

The photochemistry and photophysics of the rhenium(I) diimine tricarbonyl complexes, *fac*-[ReI(bpy)$(CO)_3$L]$^{n+}$ (bpy = 2,2′-bipyridine, L = various monodentate ligands, n = 0, 1), have attracted a lot of interests since they show emissions in good quantum yields even in solution at ambient temperature[1] and can play a role as a photocatalyst for CO_2 reduction.[2,3] The electronic states of these complexes are characterised by 5d orbitals of the rhenium atom (d^6 metal ion) and low-lying □ and □* orb

the charge-transfer (CT), ligand-centered (LC), and metal-centered (MC) states appear as low-lying electronic excited states in their photochemistry. Detailed understanding of their energetics and dynamics is important to design new photo-functional materials. Triplet metal-to-ligand charge-transfer (^{3}MLCT) states have been mostly studied over the last three decades, because such emissions or photo-catalytic activities are closely related to the lowest ^{3}MLCT state.[4] The ^{3}MLCT state cannot be optically accessed from the electronic ground state, which is a singlet state herein, while the initial photoactivation of the rhenium(I) complexes is of singlet metal-to-ligand charge-transfer (^{1}MLCT) character. The ^{3}MLCT state should be populated via the intersystem crossing (ISC) between the singlet and triplet states and the internal conversion (IC) of the singlet-singlet or triplet-triplet states. Such a decay process can be achieved in several hundreds of femtoseconds.[5-7]

The complex with a halide ligand, e.g. *fac*-[Re^{I}(bpy)$(CO)_3$Cl], is thermally and photochemically robust under low-energy ultraviolet (UV) light (▱> 330 nm).[8-10] On the other hand, the complex with a phosphorus ligand, e.g. *fac*-[Re^{I}(bpy)$(CO)_3P(OEt)_3]^+$ (Et = CH_2CH_3), is photoactive; it shows the photochemical ligand substitution (PLS) reactions (Scheme 1) in which the axial CO ligand is substituted by a solvent molecule, e.g. CH_3CN

(acetonitrile).[11,12] The PLS is a typical reaction that proceeds via the ^{3}MC state of d^6 metal complexes, which can be understandable qualitatively by the conventional ligand-field theory.[13] Ishitani and co-workers have proposed the following mechanisms (Scheme 2) from their experimental results:[11,14]

a) Of the phosphorus complexes, the ^{3}MC state is energetically accessible from the ^{3}MLCT state and the potential energy surface of the ^{3}MC state is repulsive along the Re-CO dissociation coordinate.

b) Of the halide complexes, the ^{3}MC state is also accessible from the ^{3}MLCT state, but there is an extra potential barrier which has a rather high activation energy for the Re-CO dissociation because of the trans effect of the ligand.

However, the mechanism of the PLS or the reason for the photostability of the halide complexes remain obscure because there are no theoretical investigations so far for the relationship between the ^{3}MLCT (or ^{1}MLCT) and ^{3}MC states, and the potential barriers in the ^{3}MC state.

In this study, the CO ligand dissociation pathway of *fac*-$[Re^{I}(bpy)(CO)_3P(OMe)_3]^+$ (Me = CH_3) - as the dominant process in the PLS reactions - has been explored by *ab initio* quantum chemistry calculations. Geometry optimisations were achieved, not only for the equilibrium structures (EQs) but also for the conical intersections (CIs) and the seams of crossing (SXs). Characterizing CI and SX is important since the IC or ISC efficiently occurs at the CI or SX, respectively.[15] Generally speaking, the geometry optimisation for a CI (or a SX) requires a computation of the non-adiabatic coupling matrix elements (NACMEs) and the complete-active-space self-consistent-field (CASSCF) method[16] or much higher levels of *ab initio* electronic structure theory can only compute the NACMEs, but the CASSCF

calculation is demanding and costly so that it cannot be applied to *fac*-[Re^{I}(bpy)$(CO)_3P(OMe)_3]^+$. With a help of the branching-plane updating method,[17] the CIs and SXs can be optimised[18] by the TD-DFT level of theory[19] which is less expensive than the CASSCF and affordable, without computing the NACMEs at all. Here we discuss the relaxation process into the ^{3}MLCT state inclusively, and then the ^{3}MLCT/^{3}MC transition, the barrier in the ^{3}MC state, the SXs to the ground state, as well. Hence, this is the first report on theoretically studied mechanisms of the PLS reactions of the rhenium(I) diimine tricarbonyl complex with a phosphorus ligand.

2. Computational details

The minima of the potential energy surfaces and the minimum energy conical intersections (MECIs) for S_3/S_2, S_2/S_1, and T_2/T_1, and the minimum energy seams of crossings (MESXs) for S_1/T_2 and T_1/S_0 were explored by the single-component artificial force induced reaction (SC-AFIR) method[20] associated with the seam model function (SMF).[21] It should be noted that the MECIs and MESXs were optimised by the branching-plane updating method[17] without computing the non-adiabatic coupling matrix element (NACME) vectors. The collision energy parameter $\square$= 150 kJ mol^{-1} was adopted in the automated search of the SC-AFIR method. The automated search was performed at the (TD-)B3LYP[23]/6-31G(d)/SDD level of calculation; the 6-31G basis set[24] was applied to H, C, N, O atoms, the 6-31G(d) to P atom,[25] and SDD (Stuttgart/Dresden) ECP basis set with quasi-relativistic effect corrections to Re atom.[26] Solvent effects of acetonitrile were considered by the conductor-like polarizable continuum model (C-PCM).[27] In this model the equilibrium solvation was taken into account. The obtained structures by the SC-AFIR search were refined at the

(TD-)B3LYP/cc-pVDZ[28]/SDD level with the C-PCM. The TD-DFT method with the B3LYP functional and the C-PCM reproduced the experimental absorption peak well for *fac*-[Re^{I}(bpy)$(CO)_3$X] (X = Cl, Br, I).[6,22] This level of theory also works in the case with *fac*-[Re^{I}(bpy)$(CO)_3P(OMe)_3]^+$ as shown below. All these calculations were computed using a developmental version of the GRRM program[29] combined with the Gaussian 09 electronic structure calculation program.[30] The spin-orbit coupling (SOC) constants were also computed by the linear response approach[31] using the Dalton 2015.1 quantum chemistry program system.[32]

3. Results and Discussion

3.1 The Excited States and the Relaxation Pathway

Table 1 shows the relative energies of the low-lying singlet (S_1, S_2, and S_3) and triplet (T_1, T_2, T_3, and T_4) electronic excited states of *fac*-[Re^{I}(bpy)$(CO)_3P(OMe)_3]^+$, and the oscillator strengths of the excitations from the ground (S_0) state as well. These electronic states are characterised by three 5d orbitals of the rhenium atom and low-lying □ and □* or

localised on the bpy ligand (Fig. 1) which is the same as *fac*-[Re^{I}(bpy)$(CO)_3$X] (X = Cl, Br, I) complexes.[6,7,22] Although the T_1 and T_3 states include the LC excitation, HOMO-3 (99*a*) → LUMO (103*a*), all of the low-lying states indicate the MLCT character between the rhenium atom and bpy moiety. It is well reported that the photoexcitation of the Re(I) diimine tricarbonyl complexes corresponds to the MLCT excitation.[6,7] The $S_3 \leftarrow S_0$ vertical excitation energy, 3.62 eV (which corresponds to 319 nm in wavelength), is in good agreement with the experimental absorption peak,[33] and its oscillator strength f = 0.1044 is sufficiently larger

than the $S_2 \leftarrow S_0$ or $S_1 \leftarrow S_0$ excitations. Then we assume the following relaxation pathway starts on the S_3 state in the Franck-Condon (FC) region.

Several important structural parameters of *fac*-$[Re^{I}(bpy)(CO)_3P(OMe)_3]^+$ optimised in the low-lying excited states are listed on Table 2. Once the $S_3 \leftarrow S_0$ photoexcitation occurs, the molecule starts moving towards the minimum (S_3-min), since the potential energy surface is downhill in the FC region. In this system the minimum-energy CI between the S_3 and S_2 states (S_3/S_2-MECI) is very close to the S_3-min and there are almost no barriers, so that the system can be easily relaxed into the S_2 state. Similarly it goes into the S_1 state through the S_2/S_1-MECI, which exists near the S_2-min, as well. Such a relaxation process has been practically understood as the Kasha's rule;[34] however, here we can characterise the pathway by optimising the minima and MECIs. In the FC region, the spin-orbit couplings between singlet and triplet states are not large enough (the coupling constants are less than 10 cm^{-1}), and internal conversions through MECIs into the S_1 state are preferable. Therefore only the intersystem crossing between the S_1 and triplet states are considered here. In the S_1 state, the spin-orbit coupling with the T_2 or T_3 state is relatively strong (the coupling constants of the S_1 with the T_1, T_2, T_3, and T_4 states are 0.89, 5.18, 5.99, and 2.55 cm^{-1}, respectively). The minimum-energy SX between the S_1 and T_2 states (S_1/T_2-MESX) is located with a barrier of 0.03 eV from the S_1-min. The S_1/T_3-MESX is also located at 0.09 eV above the S_1-min, but, the main exit from the S_1 state would be the S_1/T_2-MESX energetically. At the S_1/T_2-MESX, the complex could undergo intersystem crossing to the T_2 state requiring no thermal activation. Then, the system relaxes into the T_1 state quickly, because the minimum of the T_2 state corresponds to a T_2/T_1-MECI. The resulting T_1 state is also the ^{3}MLCT state (102*a* →

103*a*, Fig. 2). This relaxation process can be compared to those for [Re(bpy)$(CO)_3$ X] (X = Cl, Br, I) complexes. Experimentally, both ^{3}MLCT and ^{3}LC states were shown to be involved in the relaxation dynamics in the case of [Re(bpy)$(CO)_3$Cl].[8] Consistently, it has been suggested theoretically that the ISC occurs to both T_2 (^{3}MLCT) and T_3 (^{3}LC) states.[6,22] It has also been shown that the ISC to the T_2 (^{3}MLCT) state is the main path, and the system finally relaxes into the T_1 (^{3}MLCT) state by internal conversions. The PLS reaction therefore occurs on the T_1 surface in both $[Re^I(bpy)(CO)_3P(OMe)_3]^+$ and [Re (bpy)$(CO)_3$Cl].

In this relaxation pathway, the deformations of molecular geometry are very small. The elongations of the Re-P, Re-C_{ax}, and Re-C_{eq} bond lengths do not exceed 0.078 Å (~3%), 0.052 Å (~3%), and 0.077 Å (~4%), respectively. The C_{eq}-Re-C_{eq} angle varies between 85.04° and 95.65°, and this is the largest change among the bond angles. These features are quite similar to [Re(bpy)$(CO)_3$X] (X = Cl, Br, I) complexes,[6] although the XLCT (halide-to-ligand CT) character is absent. The XLCT character might contribute to lower energy levels of the excited states in [Re(bpy)$(CO)_3$Cl] system by 0.2 - 0.5 eV.

3.2 Mechanism of the Photochemical Ligand Substitution (PLS) Reaction

After the photoexcitation and the ISC between the singlet and triplet states, the *fac*-$[Re^I(bpy)(CO)_3P(OMe)_3]^+$ relaxes to the T_1 state, which is the ^{3}MLCT. As described above, the PLS is a typical reaction that proceeds via the MC state of d^6 metal complexes, but no crossings of MLCT/MC states appeared on the relaxation path. Ishitani and co-workers[11] reported the *fac*-$[Re^I(bpy)(CO)_3P(OMe)_3]^+$ shows an emission (λ_{max} = 543 nm, Φ_{em} = 0.216) with 1 μs of lifetime, and also the PLS reaction (Φ_{PLS} = 0.118) competes with the emission. Their experimental results strongly suggested 1) the PLS reaction occurs via a ^{3}MC

state which is thermally accessible from the ^{3}MLCT state, and 2) the axial CO (CO_{ax}) is selectively dissociated but any equatorial COs (CO_{eq}) are not. From these points of view, the reactivity for the PLS reaction can be characterised by the topology of the T_1 surface along the Re-CO_{ax} dissociation coordinate, and the character of the T_1 state would change from ^{3}MLCT to ^{3}MC.

In this study a local minimum on the T_1 potential energy surface, at which the Re-C_{ax} is lengthened by 0.177 Å and the Re-C_{ax}-O_{ax} angle is bent by 49.30°, was found (T_1-min (bent)). At the T_1-min (bent) the singly occupied molecular orbitals (SOMOs) consist mostly of the 5d orbitals (Fig. 3), so that the character of the T_1 state changes from the ^{3}MLCT to the ^{3}MC. Also the transition state (TS) between the T_1-min (global) and T_1-min (bent) was optimised. It corresponds to a critical point of the ^{3}MLCT/^{3}MC states. The TD-DFT calculation supports that this is an avoided crossing between the T_1 and T_2 states. On the ^{3}MC state the low-energy barrier, 0.17 eV (16.08 kJ mol^{-1}) above the T_1-min (bent), exists as a TS along the Re-CO_{ax} dissociation coordinate (T_1-TS (dissociation)). Some of the structural parameters are summarised in Table 3, and the energy profile is depicted in Fig. 4 (a).

To evaluate whether the B3LYP functional and C-PCM model describes the relative energy between the MLCT and MC states properly, the kinetic data is calculated and it is compared with the experimental data.[11] The overall PLS reaction rate constant k'_r can be written by the rate constants for elementary steps, k_{th} (T_1-min (global) → T_1-TS (bent)), k_{-th} (T_1-TS (bent) → T_1-min (global)), and k_r (T_1-TS (bent) → T_1-TS (dissociation)). Once the CO ligand leaves it is assumed that no CO ligand returns to the T_1-min (bent), so that k_{-r} (T_1-TS (dissociation) →

T_1-TS (bent)) to be zero. Then the overall PLS reaction rate constant k'_r based on the steady state approximation is

$$k'_r = (k_{th} \cdot k_r) / (k_{th} + k_{-th} + k_r) \quad (1)$$

and the overall free energy barrier ($\Delta G_r'$) can be calculated as

$$\Delta G'_r \approx -\ln k'_r \cdot RT \quad (2)$$

where R is the gas constant and T is the temperature. The calculated relative free energies at 298 K at the T_1-min (global), T_1-TS (bent), T_1-min (bent), and T_1-TS (dissociation) are 2.619, 2.945, 2.915, and 2.970 eV, respectively. So that the rate constants k_{th}, k_{-th}, and k_r are 1.22×10^8, 1.26×10^{14}, and 4.52×10^{12} s^{-1}, respectively. Consequently the overall reaction rate constant k'_r and the free energy barrier $\Delta G_r'$ can be calculated as 4.23×10^6 s^{-1} and 3323 cm^{-1}. The experimentally reported free energy barrier at 298 K ($\Delta G^{\ddagger}_{298}$) is 3740 ± 760 cm^{-1}. Here, the B3LYP functional was successful in describing these MLCT and MC states.

In contrast to *fac*-$[Re^I(bpy)(CO)_3P(OMe)_3]^+$, the rhenium diimine tricarbonyl complex with halide ligand *fac*-$[Re^I(bpy)(CO)_3Cl]$ is photostable and no PLS reaction is observed.[11,12] What does control reactivity for the PLS reaction? We have explored the Re-CO_{ax} dissociation pathway of *fac*-$[Re^I(bpy)(CO)_3Cl]$ and the structural parameters are summarised in Table 4, and the energy profile is depicted in Fig. 4 (b). As well as *fac*-$[Re^I(bpy)(CO)_3P(OMe)_3]^+$, the minimum in the ^{3}MC state, at which the Re-C_{ax} is lengthened by 0.127 Å and the Re-C_{ax}-O_{ax} angle is bent by 50.69°, was found. There is a barrier of 0.378 eV (36.47 kJ mol^{-1}) to the Re-CO_{ax} dissociation. The barrier is substantially higher than that in the case of *fac*-$[Re^I(bpy)(CO)_3P(OMe)_3]^+$ (16.08 kJ mol^{-1}). Mixing of the XLCT (halide-to-ligand CT) character might contribute to lower energy levels of the MLCT

state. In contrast, there is no mixing of the XLCT character to the MC state, so that the barrier becomes rather large. This would be one reason of the low PLS reactivity of *fac*-[Re^{I}(bpy)$(CO)_3$Cl].

Another important factor determining the PLS reactivity would be the efficiency of the ISC to the S_0 state. The T_1/S_0-MESXs were therefore searched by the SC-AFIR method. The search found 11 independent T_1/S_0-MESXs for *fac*-[Re^{I}(bpy)$(CO)_3$Cl]. Fig. 5 shows the four lowest T_1/S_0-MESXs. All of these MESXs have lower energy than 3.20 eV, the T_1-TS (dissociation). The second and third lowest-energy T_1/S_0-MESXs, especially, are located at 3.05 and 3.06 eV (Fig. 5 (ii) and (iii)) respectively on the way from T_1-min (global) to T_1-min (bent), so that these MESXs are important for the reaction mechanism. Therefore *fac*-[Re^{I}(bpy)$(CO)_3$Cl] would prefer to relax into the S_0 state in the FC region than overcoming the barrier for the PLS reaction energetically. The T_1/S_0-MESXs, in which the bipyridine ring is distorted, are located above 3.70 eV (see Electronic Supplementary Information for details) and rather higher than the barriers.

The SC-AFIR search for the T_1/S_0-MESXs of *fac*-[Re^{I}(bpy)$(CO)_3P(OMe)_3]^+$ was also performed. In our search 23 independent structures of the T_1/S_0-MESXs were obtained. The lowest four T_1/S_0-MESXs are depicted in Fig. 6 and they are very similar to those of *fac*-[Re^{I}(bpy)$(CO)_3$Cl] (Fig. 5), except the MESX after the CO_{eq} dissociation (at 3.34 eV). However, all of these MESXs are located at higher energy than 3.22 eV of the T_1-TS (dissociation). On the Re-CO_{ax} dissociation coordinate the MESXs at 3.45 and 3.50 eV (Fig. 6 (iii) and (iv)) would be most effective, but the TS for the PLS reaction has much lower energy, then the PLS reaction is energetically preferred. In addition, the spin-orbit coupling (SOC) constant at the T_1/S_0-MESX computed by the linear response theory[31] is 2.55 cm^{-1}

(Fig. 6(iii)), and that of *fac*-[Re^{I}(bpy)$(CO)_3$Cl] is 47.8 cm^{-1} (Fig. 5(ii)). This supports *fac*-[Re^{I}(bpy)$(CO)_3P(OMe)_3]^+$ relaxes much slower than *fac*-[Re^{I}(bpy)$(CO)_3$Cl] through the T_1/S_0-MESX, so that more probabilities of the PLS reaction are expected in *fac*-[Re^{I}(bpy)$(CO)_3P(OMe)_3]^+$. From the viewpoint of the efficiencies of the dissociation on the T_1 and of the decay to the S_0, the reactivity is explained successfully.

3.3 Selectivity of CO Position on the PLS Reaction

The rhenium tricarbonyl complex has three carbonyl ligands, an axial and two equatorial COs. Only the dissociation pathway for CO_{ax} has been discussed above since the ^{13}C-NMR study has revealed that any CO_{eq} are not dissociated.[11] In this study, however, the transition state structures towards the PLS reaction have been searched by the SC-AFIR method, not only for CO_{ax} but also for CO_{eq}.

The important points in the Re-CO_{eq} dissociation pathways of *fac*-[Re^{I}(bpy)$(CO)_3P(OMe)_3]^+$ and *fac*-[Re^{I}(bpy)$(CO)_3$Cl] are depicted in Figure 4 as well as that of the Re-CO_{ax}. The structural parameters are also summarised in Table 5 and Table 6. In the same way as the Re-CO_{ax} dissociation pathway, it is characterised by bending of the CO_{eq}. However, the (T_1-TS (dissociation))$_{eq}$ is located at much higher energy than the (T_1-TS (dissociation))$_{ax}$ and the S_0/T_1-MESXs, so that the Re-CO_{ax} dissociation is energetically preferable. Note that the T_1-TS (bent) would exist as a T_2/T_1-MECI because the character of the state is interchanged between the ^{3}MLCT and ^{3}MC. In this study, the (T_1-TS (bent))$_{eq}$ is obtained as the T_2/T_1-MECI.

Conclusions

In this article, the mechanism of the CO ligand dissociation of

fac-[Re^{I}(bpy)$(CO)_3P(OMe)_3]^+$ has theoretically been investi-gated, as the dominant process of the photochemical ligand substitution (PLS) reactions of *fac*-[Re^{I}(bpy)$(CO)_3PR_3]^+$. The excited states have been calculated by the TD-DFT method with the B3LYP functional. The experimentally observed absorption peak was assigned to the S_3 (^{1}MLCT) ← S_0 (ground) photoexcitation. Once the photoexcitation occurrs, the system is able to decay into the S_1 and T_1 states through conical intersections and seam of crossings with sufficiently low energy barriers, and the molecular geometry does not change so much. The relaxation is achievable within the Franck-Condon (FC) region. Such a fast decay process of *fac*-[Re^{I}(bpy)$(CO)_3$ $P(OMe)_3]^+$ is quite similar to that of photostable *fac*-[Re^{I}(bpy) $(CO)_3$Cl]. The PLS reactivity can be determined by the topology of the T_1 potential energy surface. Around the FC region the T_1 state has a character of the metal-to-ligand charge-transfer (^{3}MLCT), and it changes to the triplet metal-centered (^{3}MC) state as the Re-CO bond is elongated and bent. Equatorial CO ligands have a much higher energy barrier to dissociate than that of the axial CO, so that the axial CO ligand selectively dissociates in the PLS reaction. Whereas both of *fac*-[Re^{I}(bpy)$(CO)_3P(OMe)_3]^+$ and *fac*-[Re^{I}(bpy)$(CO)_3$Cl] have similar energy profiles along the coordinate of the Re-CO dissociation, *fac*-[Re^{I}(bpy)$(CO)_3$Cl] is photostable and it shows no PLS reactivity. It is shown that the axial CO dissociation barrier on the T_1 state is substantially higher in *fac*-[Re^{I}(bpy)$(CO)_3$Cl] than that in *fac*-[Re^{I}(bpy)$(CO)_3P(OMe)_3]^+$. Furthermore, the single-component artificial force induced reaction (SC-AFIR) search reveals that the minimum-energy seam of crossings between the T_1 and S_0 states (T_1/S_0-MESXs) exist before and below the barrier in the *fac*-[Re^{I}(bpy)$(CO)_3$Cl] system, while all T_1/S_0-MESXs exist before and above the barrier in *fac*-[Re^{I}(bpy)$(CO)_3P(OMe)_3]^+$ (Scheme 3). Therefore *fac*-[Re^{I}(bpy)$(CO)_3$Cl] can decay into the S_0 state and it shows no

PLS reactions.

Acknowledgements

The authors would like to thank Dr. Chantal Daniel of Université de Strasbourg for stimulating discussions. This work is supported by a grant from Japan Science and Technology Agency with a Core Research for Evolutional Science and Technology (CREST) in the Area of “Establishment of Molecular Technology towards the Creation of New Functions”. In this work we used the supercomputer of ACCMS, Kyoto University, Japan.

References

1 M. Wrighton and D. L. Morse, *J. Am. Chem. Soc.*, 1974, **96**, 998-1003.

2 J. Hawecker, J.-M. Lehn and R. Ziessel, *Helv. Chim. Acta*, 1986, **69**, 1990-2012.

3 H. Takeda, K. Koike, H. Inoue and O. Ishitani, *J. Am. Chem. Soc.*, 2008, **130**, 2023-2031.

4 A. Vlček, Jr., *Top. Organomet. Chem.*, 2010, **29**, 73-114.

5 A. Cannizzo, A. M. Blanco-Rodríguez, A. E. Nahhas, J. Šebera, S. Záliš, A. Vlček, Jr. and M. Chergui, *J. Am. Chem. Soc.*, 2008, **130**, 8967-8974.

6 C. Gourlaouen, J. Eng, M. Otsuka, E. Gindensperger and C. Daniel, *J. Chem. Theory Comput.*, 2015, **11**, 99-110.

7 J. Eng, C. Gourlaouen, E. Gindensperger and C. Daniel, *Acc. Chem. Res.*, 2015, **48**, 809-817.

8 S. Sato, Y. Matubara, K. Koike, M. Falkenström, T. Katayama, Y. Ishibashi, H. Miyasaka, S. Taniguchi, H. Chosrowjan, N. Mataga, N. Fukuzawa, S. Koshihara, K. Onda and O. Ishitani, *Chem. Eur. J.*, 2012, **18**, 15722-15734.

9 S. Sato, A. Sekine, Y. Ohashi, O. Ishitani, A. M. Blanco-Rodríguez, A. Vlček, T. Unno

and K. Koike, *Inorg. Chem.*, 2007, **46**, 3531-3540.

10 S. Sato, T. Morimoto and O. Ishitani, *Inorg. Chem.*, 2007, **46**, 9051-9053.

11 K. Koike, N. Okoshi, H. Hori, K. Takeuchi, O. Ishitani, H. Tsubaki, I. P. Clark, M. W. George, F. P. A. Johnson and J. J. Turner, *J. Am. Chem. Soc.*, 2002, **124**, 11448-11455.

12 K. Koike, J. Tanabe, S. Toyama, H. Tsubaki, K. Sakamoto, J.R. Westwell, F.P.A. Johnson, H. Hori, H. Saitoh, O. Ishitani, *Inorg. Chem.*, 2000, **39** 2777-2783.

13 C. L. Ballhausen, *Introduction to Ligand Field Theory*, McGraw-Hill Book Company, Inc., New York NY, 1962.

14 S. Sato and O. Ishitani, *Coord. Chem. Rev.*, 2015, **282-283**, 50-59.

15 D. R. Yarkony, *J. Phys. Chem.*, 1999, **103**, 6658-6668.

16 P. G. Szalay, T. Müller, G. Gidofalvi, H. Lischka and R. Shepard, *Chem. Rev.* 2012, **112**, 108-181.

17 S. Maeda, K. Ohno and K. Morokuma, *J. Chem. Theory Comput.*, 2010, **6**, 1538-1545.

18 S. Maeda, Y. Harabuchi, T. Taketsugu and K. Morokuma, *J. Phys. Chem. A*, 2014, **118**, 12050-12058.

19 R. Bauernschmitt and R. Ahlrichs, *Chem. Phys. Lett.*, 1996, **256**, 454-464.

20 S. Maeda, T. Taketsugu and K. Morokuma, *J. Comput. Chem.*, 2014, **35**, 166-173.

21 S. Maeda, K. Ohno and K. Morokuma, *J. Phys. Chem. A*, 2009, **113**, 1704-1710.

22 Y. Harabuchi, J. Eng, E. Gindensperger, T. Taketsugu, S. Maeda and C. Daniel, *J. Chem. Theory Comput.*, 2016, **12**, 2335-2345.

23 A. D. Becke, *J. Chem. Phys.*, 1993, **98**, 5648-5652; C. Lee, W. Yang and R. G. Parr, *Phys. Rev. B*, 1988, **37**, 785-789.

24 R. Ditchfield, W. J. Hehre and J. A. Pople, *J. Chem. Phys.*, 1971, **54**, 724-728; W. J.

Hehre, R. Ditchfield and J. A. Pople, *J. Chem. Phys.*, 1972, **56**, 2257-2261.

25 M. M. Francl, W. J. Pietro, W. J. Hehre, J. S. Binkley, M. S. Gordon, D. J. DeFrees and J. A. Pople, *J. Chem. Phys.*, 1982, **77**, 3654-3665.

26 D. Andrae, U. Häußermann, M. Dolg, H. Stoll and H. Preuß, *Theor. Chim. Acta*, 1990, **77**, 123-141.

27 M. Cossi, N. Rega, G. Scalmani and V. Barone, *J. Comput. Chem.*, 2003, **24**, 669-681.

28 T. H. Dunning, Jr., *J. Chem. Phys.*, 1989, **90**, 1007-1023; D. E. Woon and T. H. Dunning, Jr., *J. Chem. Phys.*, 1993, **98**, 1358-1371.

29 S. Maeda, Y. Harabuchi, Y. Sumiya, M. Takagi, M. Hatanaka, Y. Osada, T. Taketsugu, K. Morokuma and K. Ohno, *GRRM program package, a developmental version ed.*, Hokkaido University, 2016, see http://grrm.chem.tohoku.ac.jp/GRRM/index_e.html.

30 M. J. Frisch, G. W. Trucks, H. B. Schlegel, G. E. Scuseria, M. A. Robb, J. R. Cheeseman, G. Scalmani, V. Barone, B. Mennucci, G. A. Petersson, H. Nakatsuji, M. Caricato, X. Li, H. P. Hratchian, A. F. Izmaylov, J. Bloino, G. Zheng, J. L. Sonnenberg, M. Hada, M. Ehara, K. Toyota, R. Fukuda, J. Hasegawa, M. Ishida, T. Nakajima, Y. Honda, O. Kitao, H. Nakai, T. Vreven, J. A. Montgomery, Jr., J. E. Peralta, F. Ogliaro, M. Bearpark, J. J. Heyd, E. Brothers, K. N. Kudin, V. N. Staroverov, T. Keith, R. Kobayashi, J. Normand, K. Raghavachari, A. Rendell, J. C. Burant, S. S. Iyengar, J. Tomasi, M. Cossi, N. Rega, J. M. Millam, M. Klene, J. E. Knox, J. B. Cross, V. Bakken, C. Adamo, J. Jaramillo, R. Gomperts, R. E. Stratmann, O. Yazyev, A. J. Austin, R. Cammi, C. Pomelli, J. W. Ochterski, R. L. Martin, K. Morokuma, V. G. Zakrzewski, G. A. Voth, P. Salvador, J. J. Dannenberg, S. Dapprich, A. D. Daniels, O. Farkas, J. B. Foresman, J. V. Ortiz, J. Cioslowski and D. J. Fox, *Gaussian 09, Revision D.01*, Gaussian Inc., Wallingford CT,

2013.

31 O. Vahtras, H. Ågren, P. Jørgensen, H. J. Aa. Jensen, T. Helgaker and J. Olsen, *J. Chem. Phys.*, 1992, **96**, 2118-2126.

32 K. Aidas, C. Angeli, K. L. Bak, V. Bakken, R. Bast, L. Boman, O. Christiansen, R. Cimiraglia, S. Coriani, J. Cukras, P. Dahle, E. K. Dalskov, T. Enevoldsen, J. J. Eriksen, B. Fernández, L. Ferrighi, H. Fliegl, L. Frediani, B. Gao, K. Hald, A. Halkier, E. D. Hedegård, C. Hättig, H. Heiberg, T. Helgaker, A. C. Hennum, H. Hettema, E. Hjertenæs, M. F. Iozzi, B. Jansik, H. J. Aa. Jensen, D. Jonsson, P. Jørgensen, M. Kamiński, J. Kauczor, S. Kirpekar, W. Klopper, S. Knecht, R. Kobayashi, H. Koch, J. Kongsted, A. Ligabue, N. H. List, O. B. Lutnæs, J. I. Melo, K. V. Mikkelsen, R. H. Myhre, C. Neiss, C. B. Nielsen, P. Norman, J. Olsen, J. M. H. Olsen, A. Osted, M. J. Packer, F. Pawlowski, M. N. Pedersen, T. B. Pedersen, P. F. Provasi, Z. Rinkevicius, E. Rudberg, T. A. Ruden, K. Ruud, P. Salek, C. C. M. Samson, A. Sánchez de Merás, T. Saue, S. P. A. Sauer, B. Schimmelpfennig, K. Sneskov, A. H. Steindal, C. Steinmann, K. O. Sylvester-Hvid, P. R. Taylor, A. M. Teale, D. P. Tew, O. Vahtras, D. J. D. Wilson and H. Ågren, *Dalton, a molecular electronic structure program, Release Dalton 2015.1*, 2014, see http://daltonprogram.org.

33 H. Hori, K. Koike, M. Ishizuka, K. Takeuchi, T. Ibusuki and O. Ishitani, *J. Organomet. Chem.*, 1997, **530**, 169-176.

34 M. Kasha, *Discuss. Faraday Soc.*, 1950, **9**, 14-19.

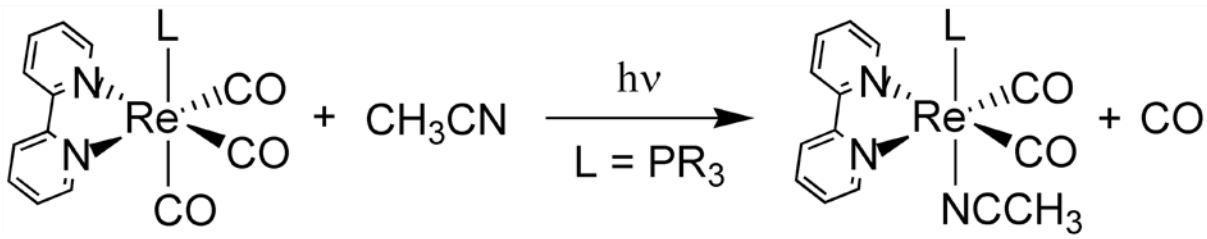

Scheme 1. Photochemical ligand substitution (PLS) reaction.

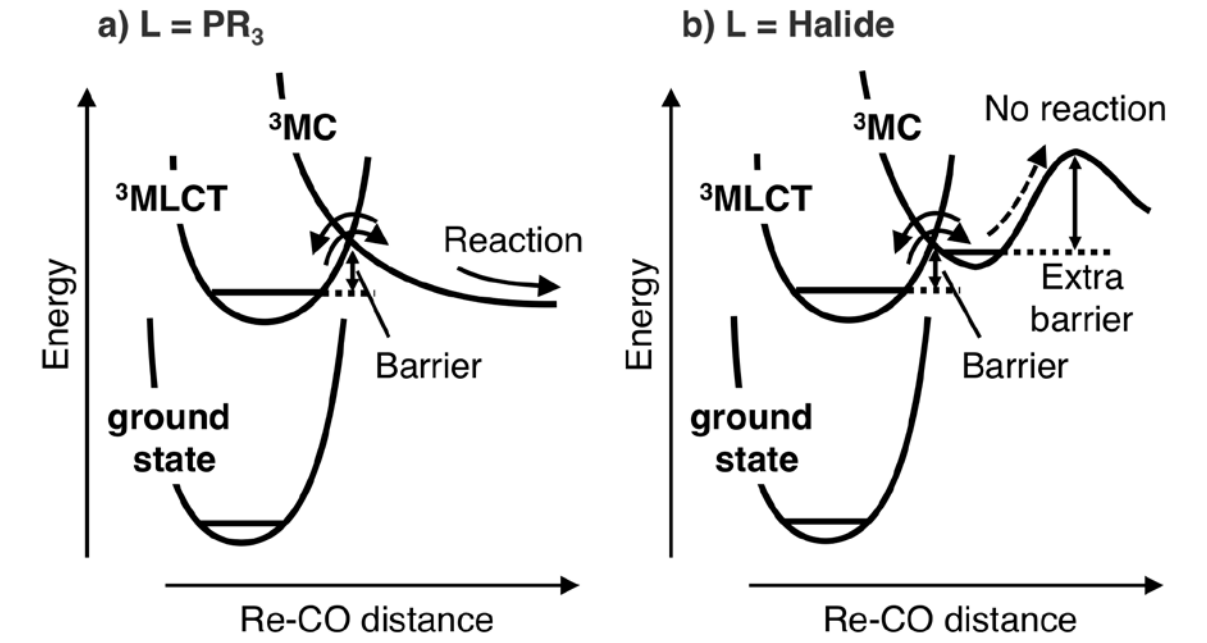

Scheme 2. Proposed mechanisms for PLS reaction (Reference 14).

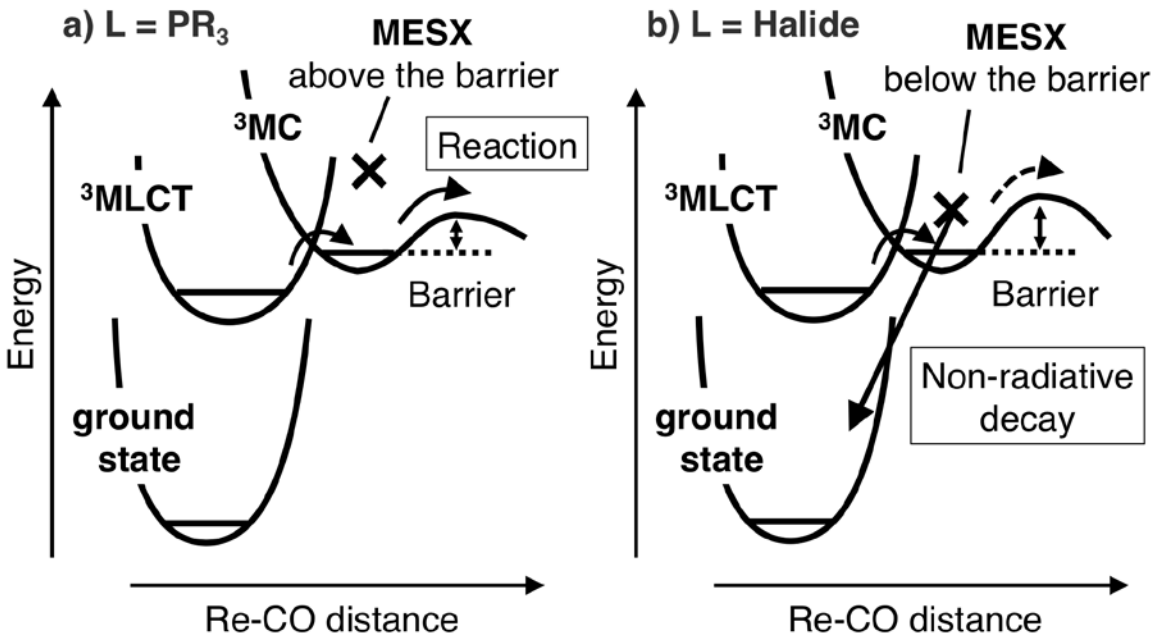

Scheme 3. Proposed mechanisms for PLS reaction from our results.

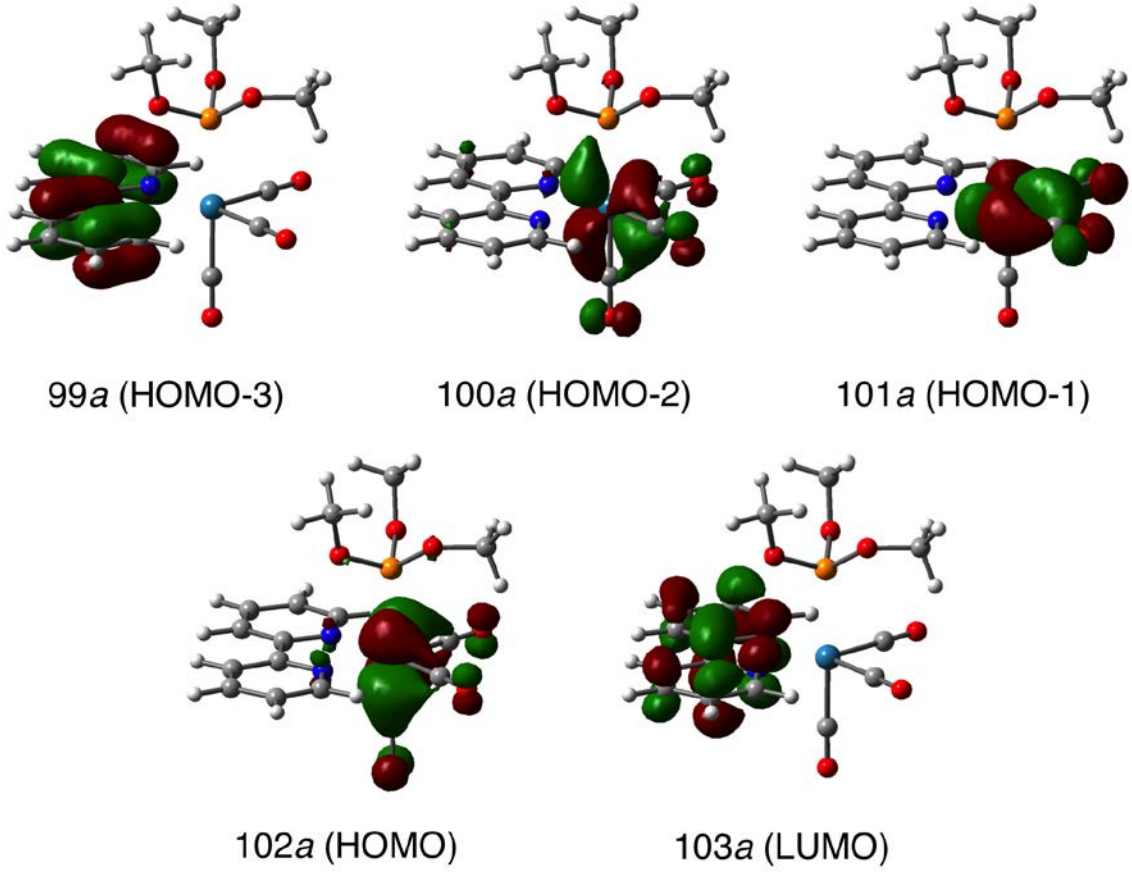

Figure 1. Frontier orbitals of *fac*-$[Re^{I}(bpy)(CO)_3P(OMe)_3]^+$ at the equilibrium structure (S_0-min).

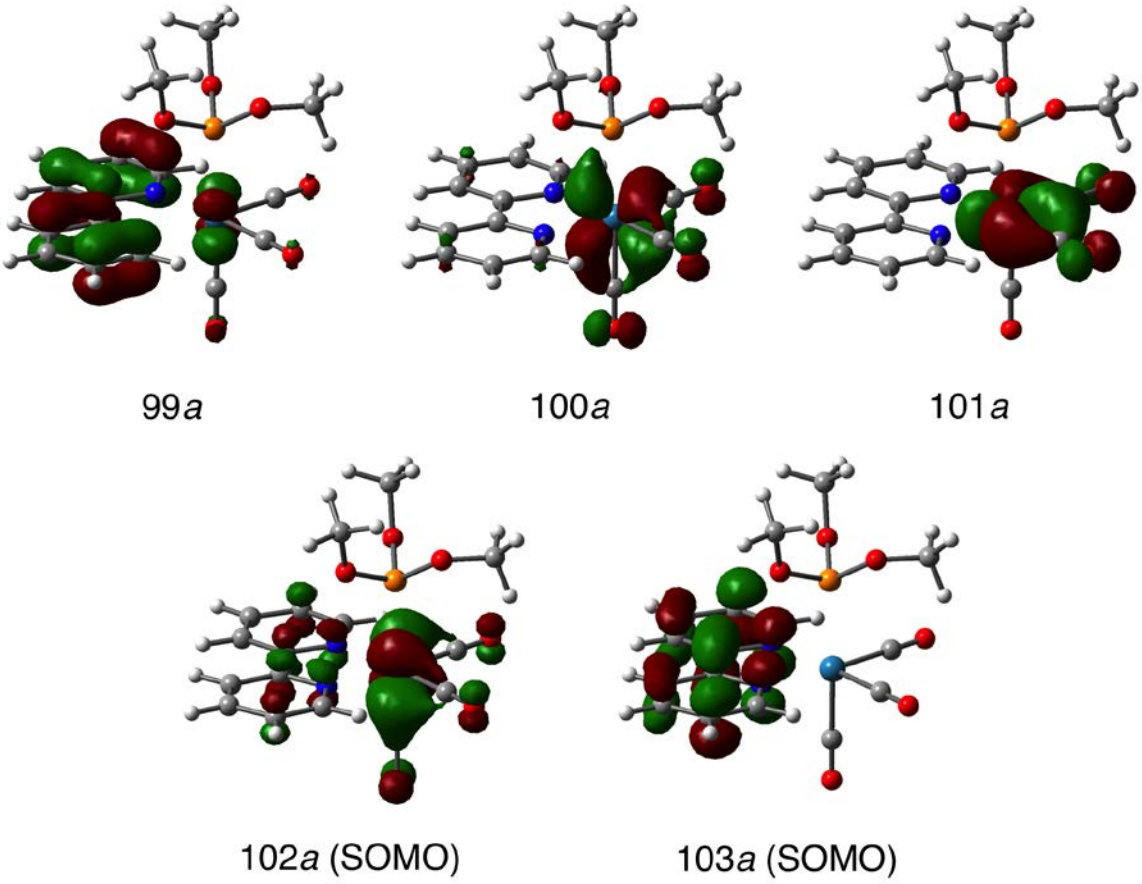

Figure 2. Frontier orbitals of *fac*-$[Re^{I}(bpy)(CO)_3P(OMe)_3]^+$ after relaxation (T_1-min).

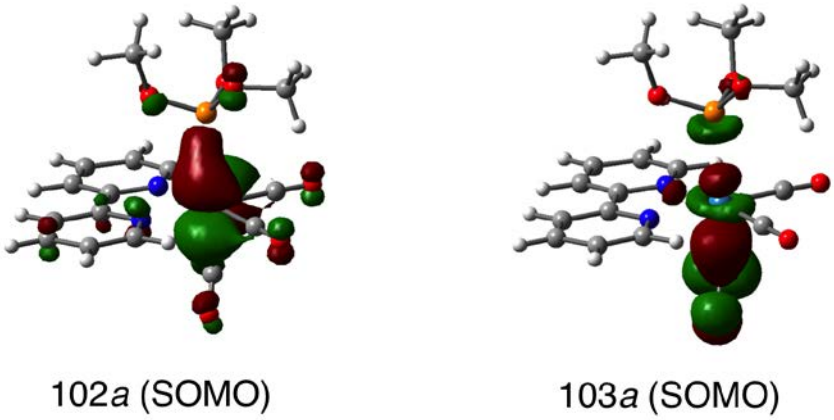

Figure 3. SOMOs of *fac*-[Re^{I}(bpy)$(CO)_3P(OMe)_3]^+$ in ^{3}MC state (T_1-min (bent)).

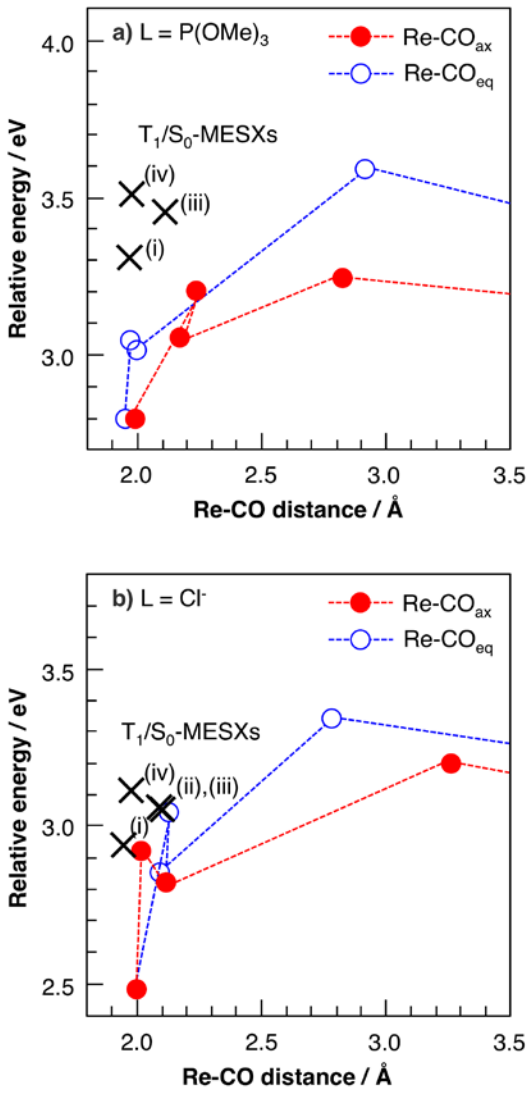

Figure 4. Potential energy profiles for Re-CO dissociation of a) *fac*-[Re^{I}(bpy)$(CO)_3$P$(OMe)_3$]$^+$ and b) *fac*-[Re^{I}(bpy)$(CO)_3$Cl]. In each panel, closed (red) and open (blue) circles indicate the points (see Table 3-7) in Re-CO_{ax} and Re-CO_{eq} dissociation paths, respectively. The lowest-energy MESXs for T_1/S_0 are indicated by cross marks (X). The labels (i) – (iv) correspond to that of the MESX structures in Figure 5 and 6.

(i) 2.939 eV

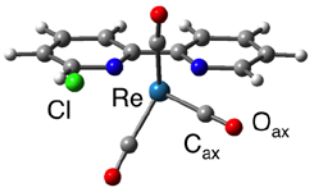

Re-Cl = 3.38 Å
Re-C_{ax} = 1.94 Å
Re-C_{ax}-O_{ax} = 178.2 °

(ii) 3.049 eV

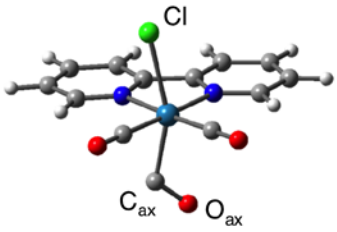

Re-Cl = 2.56 Å
Re-C_{ax} = 2.11 Å
Re-C_{ax}-O_{ax} = 119.4 °

(iii) 3.063 eV

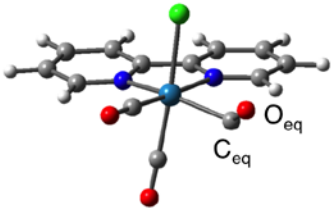

Re-Cl = 2.44 Å
Re-C_{eq} = 2.10 Å
Re-C_{eq}-O_{eq} = 123.4 °

(iv) 3.114 eV

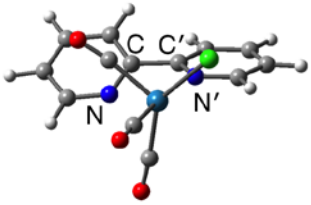

Re-Cl = 2.51 Å
Re-C_{eq} = 1.98 Å
N-C-C′-N′ = 29.5 °

Figure 5. The four lowest-energy T_1/S_0-MESXs of *fac*-[Re^{I}(bpy)$(CO)_3$Cl].

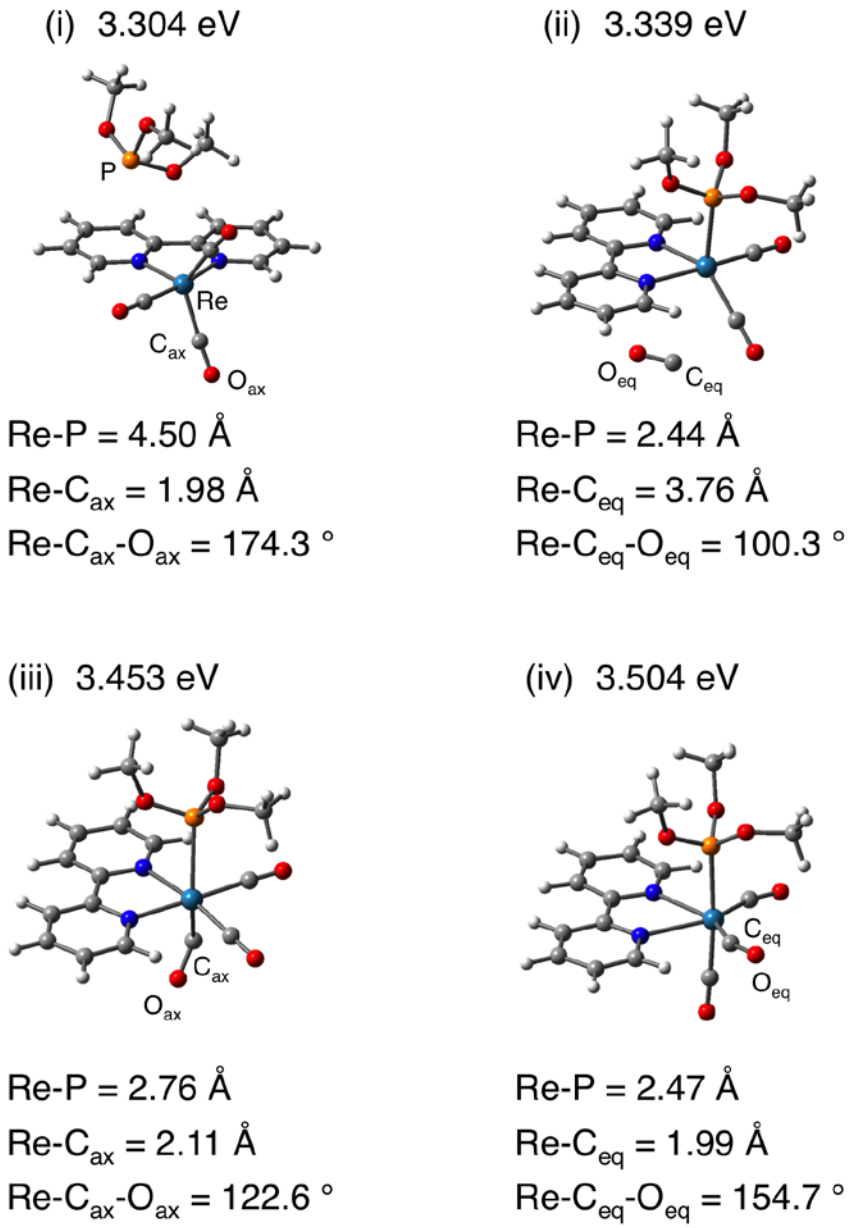

Figure 6. The four lowest-energy T_1/S_0-MESXs of *fac*-[Re^{I}(bpy)$(CO)_3$-P$(OMe)_3$]$^+$.

Table 1. Low-lying singlet and triplet states of *fac*-[Re^{I}(bpy)$(CO)_3P(OMe)_3]^+$ in the FC region.

State	Character (orbitals, weight)	λ_{abs} [eV (nm)]	Oscillator Strength *f*	$\lambda_{abs, exp}$ [nm][33]
T_1	LC (99*a*→103*a*, 49%) MLCT (102*a*→103*a*, 33%)	2.96 (419)		
T_2	MLCT (100*a*→103*a*, 80%)	3.31 (374)		
T_3	MLCT (102*a*→103*a*, 57%) LC (99*a*→103*a*, 37%)	3.41 (364)		
S_1	MLCT (102*a*→103*a*, 99%)	3.44 (360)	0.0010	(348^{sh})
T_4	MLCT (101*a*→103*a*, 91%)	3.44 (357)		
S_2	MLCT (101*a*→103*a*, 97%)	3.47 (342)	0.0004	(348^{sh})
S_3	MLCT (100*a*→103*a*, 96%)	3.62 (319)	0.1044	318

* *sh* : shoulder peak

Table 2. Optimised structural parameters of *fac*-[Re^{I}(bpy)$(CO)_3P(OMe)_3]^+$. The optimised parameters at the S_0-min (global minimum) are listed as that of the S_3 state in the Franck-Condon (FC) region. The B3LYP/cc-pVDZ/SDD level of calculation was used to optimise the S_0-min, and the other minima were optimised by the TD-B3LYP calculation. Due to mixing of the electronic states, the S_3-min and T_2-min exist in the S_3/S_2 or T_2/T_1 conical intersections respectively.

	S_3 (FC)	(S_3-min)	S_3/S_2-MECI	S_2-min	S_2/S_1-MECI	S_1-min
	MLCT	MLCT	MLCT/MLCT	MLCT	MLCT/MLCT	MLCT
Relative Energy [eV]	3.624	3.257	3.257	3.124	3.127	3.013
Re-P [Å]	2.477	2.526	2.526	2.500	2.499	2.516
Re-N [Å]	2.225	2.172	2.172	2.163	2.168	2.159
Re-C_{ax} [Å]	1.980	2.019	2.019	1.992	1.986	2.032
Re-C_{eq} [Å]	1.947	1.987	1.987	2.022	2.024	1.997
C-C_{bpy} [Å]	1.479	1.433	1.433	1.426	1.427	1.424
N-Re-N [°]	73.97	76.73	76.73	76.06	75.93	75.86
C_{eq}-Re-C_{eq} [°]	90.37	95.14	95.14	89.87	90.54	85.04
P-Re-C_{ax} [°]	177.71	176.29	176.29	174.57	174.37	171.82
N-Re-P [°]	86.73	87.64	87.64	85.48	85.37	85.88

(Table 2. Continued)

	S_1-min	S_1/T_2-MESX	(T_2-min)	T_2/T_1-MECI	T_1-min
	MLCT	MLCT/MLCT	MLCT	MLCT/MLCT	MLCT
Relative Energy [eV]	3.013	3.046	3.005	3.005	2.553
Re-P [Å]	2.516	2.524	2.555	2.555	2.487
Re-N [Å]	2.159	2.156	2.151	2.151	2.198
Re-C_{ax} [Å]	2.032	2.031	2.004	2.004	1.985
Re-C_{eq} [Å]	1.997	1.995	1.985	1.985	1.953
C-C_{bpy} [Å]	1.424	1.428	1.433	1.433	1.394
N-Re-N [°]	75.86	76.78	76.90	76.90	75.50
C_{eq}-Re-C_{eq} [°]	85.04	88.91	95.65	95.65	89.79
P-Re-C_{ax} [°]	171.82	174.55	171.07	171.07	176.59
N-Re-P [°]	85.88	86.33	90.68	90.68	86.23

Table 3. Optimised structural parameters of *fac*-[Re^{I}(bpy)$(CO)_3P(OMe)_3]^+$ along Re-CO_{ax} dissociation coordinate by the UB3LYP/cc-pVDZ/SDD level of theory.

	T_1-min (global)[a]	T_1-min (global)	T_1-TS (bent)	T_1-min (bent)	T_1-TS (disso-ciation)
	MLCT	MLCT	MLCT/MC	MC	MC
Relative Energy [eV]	2.553	2.797	3.200	3.056	3.222
Re-P [Å]	2.487	2.490	2.449	2.539	2.435
Re-N [Å]	2.198	2.189	2.143	2.231	2.160
Re-C_{ax} [Å]	1.985	1.988	2.235	2.165	2.809
Re-C_{eq} [Å]	1.953	1.956	1.981	1.977	1.977
C-C_{bpy} [Å]	1.394	1.389	1.446	1.476	1.469
N-Re-N [°]	75.50	75.61	76.55	74.26	75.46
C_{eq}-Re-C_{eq} [°]	89.79	89.75	84.08	83.32	83.94
P-Re-C_{ax} [°]	176.59	177.51	173.42	159.80	167.79
N-Re-P [°]	179.13	179.23	146.72	129.93	127.92

[a] Optimised by the TD-B3LYP calculation.

Table 4. Optimised structural parameters of *fac*-[Re^{I}(bpy)$(CO)_3$Cl] along Re-CO_{ax} dissociation coordinate by the UB3LYP/cc-pVDZ/SDD level of theory.

	S_2-FC	T_1-min (global)	T_1-TS (bent)	T_1-min (bent)	T_1-TS (disso-ciation)
	MLCT	MLCT	MLCT/MC	MC	MC
Relative Energy [eV]	2.985	2.484	2.920	2.822	3.200
Re-Cl [Å]	2.560	2.465	2.611	2.569	2.492
Re-N [Å]	2.221	2.156	2.174	2.197	2.183
Re-C_{ax} [Å]	1.923	1.992	2.016	2.117	3.257
Re-C_{eq} [Å]	1.938	1.995	1.955	1.955	1.940
C-C_{bpy} [Å]	1.480	1.421	1.464	1.478	1.471
N-Re-N [°]	74.03	76.75	74.31	74.24	74.67
C_{eq}-Re-C_{eq} [°]	89.25	85.02	83.94	83.15	81.56
Re-C_{ax}-O_{ax} [°]	179.97	179.60	151.88	128.83	117.22
Cl-Re-C_{ax} [°]	176.57	176.12	160.61	166.99	170.00

Table 5. Optimised structural parameters of *fac*-[Re^{I}(bpy)$(CO)_3P(OMe)_3]^+$ along Re-CO_{eq} dissociation coordinate by the UB3LYP/cc-pVDZ/SDD level of theory.

	T_1-min (global)	T_1-TS (bent)	T_1-min (bent)	T_1-TS (disso-ciation)
	MLCT	MLCT/MC	MC	MC
Relative Energy [eV]	2.797	3.041	3.010	3.590
Re-P [Å]	2.490	2.476	2.468	2.477
Re-N [Å]	2.189	2.388	2.388	2.231
Re-C_{ax} [Å]	1.988	1.978	1.980	1.966
Re-C_{eq} [Å]	1.956	1.988	1.987	2.816
C-C_{bpy} [Å]	1.389	1.480	1.480	1.476
N-Re-N [°]	75.61	68.00	67.83	72.83
C_{eq}-Re-C_{eq} [°]	89.75	112.55	113.86	76.87
Re-C_{ax}-O_{ax} [°]	178.66	159.66	161.36	116.90
P-Re-C_{eq} [°]	91.33	94.66	91.16	98.29

Table 6. Optimised structural parameters of *fac*-[Re^{I}(bpy)$(CO)_3$Cl] along Re-CO_{eq} dissociation coordinate by the UB3LYP/cc-pVDZ/SDD level of theory.

	T_1-min (global)	T_1-TS (bent)[a]	T_1-min (bent)	T_1-TS (disso-ciation)
	MLCT	MLCT/MC	MC	MC
Relative Energy [eV]	2.484	3.064	2.860	3.340
Re-Cl [Å]	2.465	2.473	2.485	2.526
Re-N [Å]	2.156	2.244	2.293	2.221
Re-C_{ax} [Å]	1.992	1.955	1.950	1.952
Re-C_{eq} [Å]	1.995	2.039	2.092	2.779
C-C_{bpy} [Å]	1.421	1.461	1.480	1.480
N-Re-N [°]	76.75	72.51	71.26	74.57
C_{eq}-Re-C_{eq} [°]	85.02	98.94	97.63	92.66
Re-C_{ax}-O_{ax} [°]	179.35	156.08	135.32	124.23
Cl-Re-C_{eq} [°]	89.97	91.77	94.25	73.77

[a] T_1-TS(bent) is obtained as the T_2/T_1-MECI by the TD-DFT calculation.